Aalborg Universitet

AALBORG UNIVERSITY
DENMARK

Design and Analysis of Robust Active Damping for LCL Filters using Digital Notch Filters

Yao, Wenli; Yang, Yongheng; Zhang, Xiaobin; Blaabjerg, Frede; Loh, Poh Chiang

Design and Analysis of Robust Active Damping for *LCL* Filters using Digital Notch Filters

Wenli Yao, *Student Member*, *IEEE*, Yongheng Yang, *Member*, *IEEE*, Xiaobin Zhang,

Frede Blaabjerg, *Fellow*, *IEEE*, and Poh Chiang Loh

Abstract — **Resonant poles of *LCL* filters may challenge the entire system stability especially in digital-controlled Pulse Width Modulation (PWM) inverters. In order to tackle the resonance issues, many active damping solutions have been reported. For instance, a notch filter can be employed to damp the resonance, where the notch frequency should be aligned exactly to the resonant frequency of the *LCL* filter. However, parameter variations of the *LCL* filter as well as the time delay appearing in digital control systems will induce resonance drifting, and thus break this alignment, possibly deteriorating the original damping. In this paper, the effectiveness of the notch filter based active damping is firstly explored, considering the drifts of the resonant frequency. It is revealed that, when the resonant frequency drifts away from its nominal value, the phase lead or lag introduced by the notch filter may make itself fail to damp the resonance. Specifically, the phase lag can make the current control stable despite of the resonant frequency drifting, when the grid current is fed back. In contrast, in the case of an inverter current feedback control, the influence of the phase lead or lag on the active damping is dependent on the actual resonant frequency. Accordingly, in this paper, the notch frequency is designed away from the nominal resonant frequency to tolerate the resonance drifting, being the proposed robust active damping. Simulations and experiments performed on a 2.2-kW three-phase grid-connected PWM inverter verify the effectiveness of the proposed design for robust active damping using digital notch filters.**

Index Terms – **Notch filter, active damping, *LCL* filter, filters, digital control, time delay, parameter variations, PWM converters.**

I. INTRODUCTION

PULSE Width Modulation (PWM) converters with *LCL* filters are widely used in grid-connected applications, as exemplified in Fig. 1(a) [1]. As a third-order system, the *LCL* filter provides significantly improved attenuation of the PWM switching harmonics with reduced overall filter volume and weight [1], [2]. Unfortunately, the *LCL* filter also introduces resonant poles that give magnitude peaks at the corresponding resonant frequencies, which is identified as being highly related to the time delay (e.g., the PWM processing and sampling delays) in digital control systems [3]-[8], possibly resulting in an unstable system [9]-[11]. A rule of thumb for the controller design has been formed, where a time delay of $1.5T_s$ ($T_s = 1/f_s$ is the sampling period with f_s being the sampling frequency) is considered [4], [8]. In that case, the stability regions (i.e., without triggering the resonance) are summarized and shown in Fig. 1(b), where either the inverter-side current or the grid-side current is fed back into the control loop and f_{res} is the resonance frequency of the *LCL* filter. It can be observed that, if the inverter-side current control (i.e., ICF – Inverter Current Feedback) is adopted, an appropriate damping control is mandatory to ensure the system stability when f_{res}/f_s is beyond 1/6; in contrast, if the grid current is fed back into the control loop (i.e., GCF – Grid Current Feedback), damping should be applied when f_{res}/f_s is lower than 1/6 [3]. In general, damping is necessary in those unstable regions shown in Fig. 1(b).

When it comes to the resonance damping of the *LCL* filter, passive damping solutions are quite straightforward at the cost of increased power losses (i.e., decreased overall efficiency) [10]. As a result, active damping schemes by modifying the control algorithm are preferred in practice [8]-[27]. Prior-art active damping strategies have been extensively developed in literature, where for instance a virtual impedance system [5], [12], a high-pass filter [13], a lead-lag network [14]-[16], an Infinity Impulse Response (IIR) digital filter [17], or the weighted-feedback current [18], [19], has been employed. However, in most cases, additional sensors are required, being the major drawback (i.e., increased cost). Following, a virtual-flux- and a filter-based active damping were proposed in [20] and [21], respectively. However, an increase in the control complexity has been observed in the former active damping solution, when it is implemented in a digital control system. In contrast, the latter one, which is accomplished by simply inserting a low-pass filter or a notch filter into the forward path of the current control loop, has become a promising active damping alternative for *LCL* filters [21]-[27]. Actually, the notch-filtering concept was initially implemented in [21], where genetic algorithms have been adopted to fine tune the notch filter. Additionally, in [22], a thorough analysis of filter-based active damping was presented, and a self-commissioning technique was proposed in [23], which can
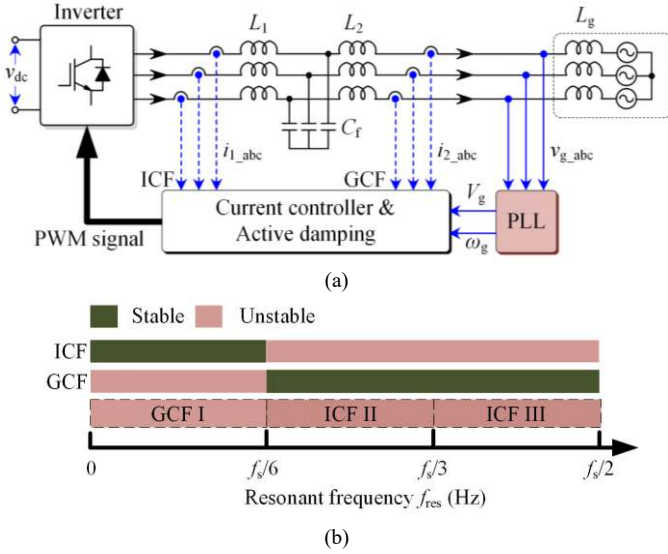
(a)

(b)

Fig. 1. Grid-connected inverter system with an *LCL*-filter considering a time delay of $1.5T_s$: (a) system schematic and overall control structure (PLL – Phase Locked Loop) and (b) stability regions, where different currents are fed back to the control loop.

TABLE I.
PARAMETERS OF THE THREE-PHASE GRID-CONNECTED PWM INVERTER WITH AN *LCL* FILTER SHOWN IN FIG. 1(A).

Parameters	Symbol	Value
Power Rating	P_n	2.2 kW
Inverter Side Inductor	L_1	1.8 mH
Grid Side Inductor	L_2	2 mH
LCL Filter Capacitor	C_f	1.5 μF, 4.7 μF, 14.1 μF
Resonant Frequency	f_{res}	4222 Hz, 2385 Hz, 1377 Hz
Grid Impedance	L_g	0~10 mH
Sampling Frequency	f_s	10 kHz
Switching Frequency	f_{sw}	10 kHz
Grid Voltage	v_g	230 V_{RMS}/50 Hz
DC Bus Voltage	V_{dc}	650 V

online estimate the resonance frequency, enabling that the notch filter can be re-tuned accordingly. Although the online estimation makes the notch filter based active damping more robust, it inevitably increases the computational burden when implemented in digital controllers. Even the aforementioned methods show strong robustness to parameter variations of the *LCL* filter, but the failure mechanism of the notch filter based active damping remains of interest for developing high-performance solutions.

In light of the above discussions, built on the work of [27], this paper firstly carries out an analysis of the traditional notch filter based active damping in terms of its sensitivity to the resonance drifting due to practical parameter variations. Accordingly, the effectiveness of the notch filter based active damping correlated to 1) the actual resonant frequency f_{res}, 2) the notch filter frequency f_n, 3) the feedback current type (i.e., ICF or GCF), and 4) the stability of single-loop controlled grid-connected inverters is discussed. It is found in the sensitivity analysis that the conventional-defined unstable regions shown in Fig. 1(b) can be further partitioned into three regions as GCF I (0~$f_s/6$), ICF II ($f_s/6$~$f_s/3$), and ICF III ($f_s/3$~$f_s/2$). When the traditional notch filter based active damping [21] is adopted, a decrease in the *LCL* resonant frequency (i.e., corresponding to a resonance drift and $f_{res} < f_n$), can maintain the stability of the current control loop only in the regions of GCF I and ICF III. This is due to a phase delay around the resonant frequency f_{res} that is introduced by the notch filter. In contrast, this phase delay may challenge the stability of the entire control loop in the region of ICF II. Furthermore, if a positive resonance drift occurs in the *LCL* filter (i.e., $f_{res} > f_n$), a phase lead introduced by the notch filter can maintain the stability of the control loop in the region of ICF II. However, in regions of GCF I and ICF III, the damping by the notch filter is not effective. Hereafter, the ICF II is accordingly identified as a compensation-demanded region, and the GCF I and ICF III are defined as delay-demanded regions.

Hence, unlike the design method proposed in [21], where the notch filter is only used to damp the resonant peak and thus the notch frequency is exactly aligned to the nominal resonant frequency, the notch frequency is placed away from the nominal resonant frequency in this paper in order to tolerate the resonance drifts. By doing so, the designed notch filter for active damping can provide sufficient phase lead or lag around the actual resonant frequency f_{res}, leading to improved robustness. Specifically, in the region of ICF II, the notch frequency is designed smaller than the *LCL* filter nominal resonant frequency for proper delay compensation. That is to say, the notch filter will behave like a phase compensator around the *LCL* filter resonant frequency. This is close to the analysis in [27]. Nevertheless, in the delay-demanded areas (i.e., GCF I and ICF III), the notch filter is assigned to introduce sufficient phase delays, when its frequency is designed beyond the LCL filter nominal resonant frequency. Doing so can pull down the phase of the open-loop system, and prevent it from crossing the $-180°$-line at the resonant frequency, and thus also contribute to a wider stability range of the active damping. Additionally, robustness analysis of the proposed active damping using digital notch filters against the *LCL* filter parameter and/or the grid impedance variations is also carried out.

The rest of this paper is organized as: § II introduces the control structure of a three-phase grid-connected system with an *LCL* filter and the traditional notch filter based active damping. In § III, the sensitivity of the traditional notch filter based active damping is addressed in the case of varying resonant frequencies due to the parameter drifting of the *LCL* filter as well as the grid impedance. Following, § IV proposes a design approach for the digital notch filter based robust active damping for *LCL* filters, where the robustness analysis of the entire closed-loop current controller considering parameter variations is also presented. Simulation and experimental results are provided in § V in order to verify the proposed notch filter based active damping method. Finally, conclusions are drawn in § VI.

II. TRADITIONAL NOTCH FILTER BASED ACTIVE DAMPING

Fig. 1(a) shows the PWM converter system considered in this paper, and the parameters of this grid-connected PWM inverter with an *LCL* filter are listed in Table I.

A. Basics of Notch Filter based Active Damping

According to the system structure shown in Fig. 1(a), the transfer-functions of the *LCL* filter in the *s*-domain from the inverter output voltage v_{inv} to the inverter output current i_1 and to the grid current i_2 can be given as

$$G_{i1}(s) = \frac{i_1(s)}{v_{inv}(s)} = \frac{(L_2+L_g)C_f s}{L_1(L_2+L_g)C_f s^2 + (L_1+L_2+L_g)s+1} \quad (1a)$$

$$G_{i2}(s) = \frac{i_2(s)}{v_{inv}(s)} = \frac{1}{L_1(L_2+L_g)C_f s^2 + (L_1+L_2+L_g)s+1} \quad (1b)$$

with

$$\omega_{res} = \sqrt{\frac{1}{C_f}\cdot\left(\frac{1}{L_1}+\frac{1}{L_2+L_g}\right)} = \sqrt{\frac{L_1+L_2+L_g}{L_1\cdot(L_2+L_g)\cdot C_f}} \quad (2)$$

where $T_s = 1/f_s$ is the sampling period with f_s being the sampling frequency and $\omega_{res} = 2\pi f_{res}$ being the resonant angular frequency of the *LCL* filter. It can be observed that the grid impedance (i.e., L_g) is also considered in the transfer-functions of (1), where a Zero-Order Hold (ZOH) is adopted for the discretization. Furthermore, the numerator of $G_{i1}(s)$ inherently has an anti-resonant peak at the frequency of:

$$\omega_0 = \sqrt{1/(L_2+L_g)C_f} \quad (3)$$

which corresponds to a small phase lag at the frequency below the resonant frequency ω_{res}. The overall *d*-axis current control structures are depicted in Fig. 2(a) and (b) for the ICF and the GCF control, respectively, in which a Proportional-Integral (PI) controller is adopted as the current controller. The PI controller can be given as

$$G_{pi}(s) = k_p\left(1+\frac{1}{T_i s}\right) \quad (4)$$

with k_p and T_i being the controller parameters given as

$$k_p = \frac{\omega_c(L_1+L_2)}{V_{dc}}, \qquad T_i = \frac{10}{\omega_c} \quad (5)$$

where V_{dc} is the DC-link voltage and ω_c is the crossover frequency.

In general, the sampling and computation process can be accounted as a time delay of δT_s [4], which is introduced in the current control system as shown in Fig. 2. Normally, δT_s is not larger than one sampling period T_s (i.e., $0<\delta<1$). In addition to the that time delay (i.e., δT_s), there is another time delay of approx. $0.5T_s$ due to the PWM processing, which can be modeled as a Zero-Order-Hold (ZOH) [4]. The PWM processing delay can then be given as

$$G_{PWM}(s) = \frac{1-e^{-sT_s}}{s} \quad (6)$$

Clearly, when assuming $\delta=1$ (corresponding to one unity delay), the total delay in the control loop will be $1.5T_s$, which is commonly used in literature for the control loop stability analysis [15]-[16], [32]-[33].

Besides, as shown in Fig. 2, a conventional notch filter is included in the control loop for active damping. The transfer function of the notch filter can be expressed as

$$G_{notch}(s) = \frac{s^2+\omega_n^2}{s^2+Qs+\omega_n^2} \quad (7)$$

in which Q is the quality factor of the notch filter determining the -3-dB rejection bandwidth, and ω_n is the notch frequency.
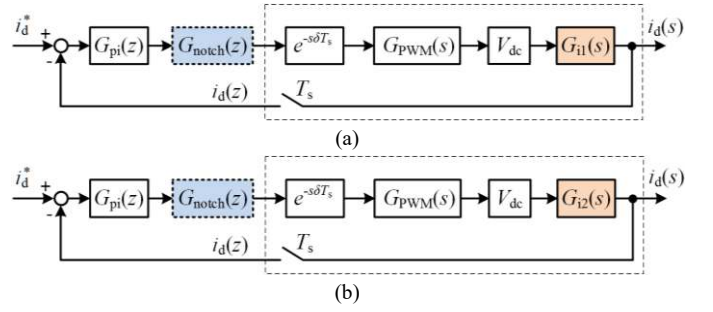

Fig. 2. Closed-loop current control system using a digital notch filter based active damping for the PWM converter with an *LCL* filter, where i_d is the *d*-axis component of the feedback current in the *dq* reference frame: (a) using inverter-side current feedback control (ICF) and (b) using grid-side current feedback control (GCF).

In [21] and [22], ω_n is exactly placed at the resonant frequency of the designed *LCL* filter (i.e., $\omega_n = \omega_{res}$) in order to cancel out the resonant peaks. Actually, this is a kind of zero-pole cancelling method, and it is very sensitive to the resonant pole variations (i.e., resonance drift) introduced by the filter parameter and unknown grid impedance changes, which will be discussed in § III.

According to Fig. 2, the open-loop transfer function of the current control system can be expressed in the *z*-domain as [4]

$$G_{open}(z) = G_{pi}(z)\cdot G_{notch}(z)\cdot Z\left\{e^{-s\delta T_s}G_{PWM}(s)\cdot V_{dc}\cdot G_i(s)\right\} \quad (8)$$

where $G_i(s)$ represents $G_{i1}(s)$ or $G_{i2}(s)$, and $G_{notch}(z)$ is the discretized notch filter according to (7). In order to verify the effectiveness of the notch filter based active damping, the filter capacitors are designed on purpose as follows. For the ICF control, C_f is chosen as 4.7 μF, which will give a resonant frequency of f_{res} = 2385 Hz, locating in the unstable area (i.e., $f_{res}/f_s > 1/6$) according to Fig. 1(b). In contrast, for the GCF control, a filter capacitance C_f of 14.1 μF will result in a resonant frequency of f_{res} =1377 Hz inside the unstable region (i.e., $f_{res}/f_s < 1/6$) as shown in Fig. 1(b). Thus, a basic analysis of the system resonance can be conducted. Fig. 3 shows the Bode plots of the *LCL* filter transfer-functions given in (1a) and (1b), the notch filter shown in (7), and the open-loop control system presented in (8), where the conventional notch filter based active damping is employed. As it is shown in Fig. 3, by placing the notch frequency exactly at the *LCL* filter resonant frequency according to the conventional design [22], the resonant peak is canceled out (i.e., not in the open-loop systems). At the same time, the phase of the *LCL* filter is compensated by the notch filter, which has a phase change of 180° (from – 90° to 90°) at its notch frequency. As a result, there is no negative − 180°-crossing with the gain above 0 dB, indicating a stable system according to the Nyquist criteria.

However, as it is shown in Fig. 3, the notch filter has a narrow rejection bandwidth and an infinite negative gain around the notch frequency. Thus, a slight error in the location of the notch frequency can contribute to a significant loss of the capability to suppress the *LCL* filter resonant peak. Especially, the notch frequency is affected by digital implementations of the notch filter [30]. In general, there are two possibilities to implement the notch filter in a digital controller. One is to design the filter in the *s*-domain, and then a discretization method is applied to the designed notch filter, resulting in a
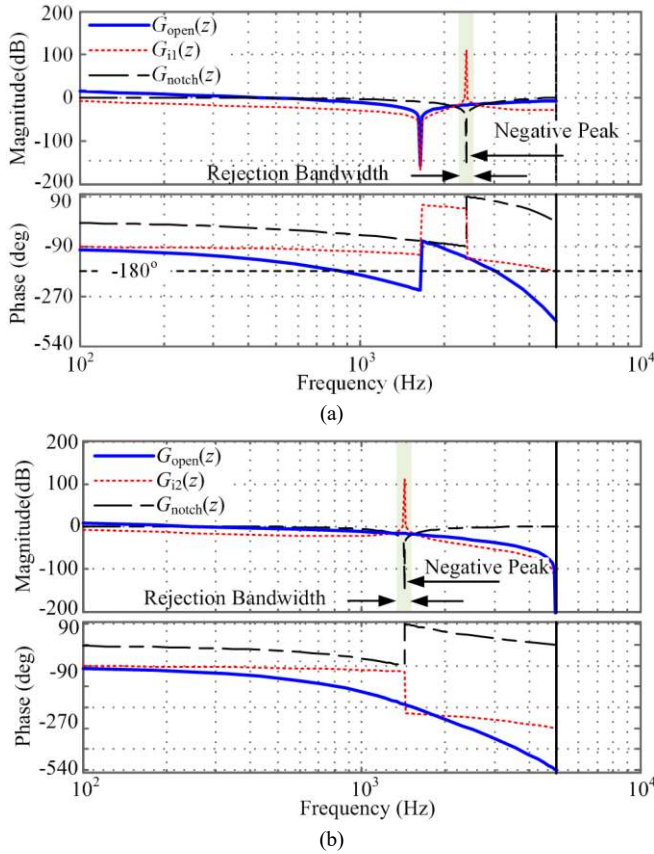
(a)

(b)

Fig. 3. Bode plots of the open-loop current controller with the traditional notch filter based active damping: (a) using the inverter-side current feedback (ICF) control and (b) using the grid-side current feedback (GCF) control.

digital notch filter (as previously achieved) [22]. Alternatively, it can be directly designed in the *z*-domain in order to reduce the phase and magnitude errors introduced by the discretization from the *s*-domain models. Since the notch frequency is sensitive to the discretization and thus the active damping performance, the following demonstrates a novel procedure to discretize the notch filter for active damping.

B. Discretization of the Notch Filter

Typically, the Tustin transformation is used to discretize the notch filter [28], and applying it to $G_{notch}(s)$ of (6) yields

$$G_{notch}(z) = G_{notch}(s)\Big|_{s=k\cdot\frac{z-1}{z+1}}$$

$$= \frac{(k^2+\omega_n^2) - 2(k^2-\omega_n^2)z^{-1} + (k^2+\omega_n^2)z^{-2}}{(k^2+\omega_n^2+kQ) - 2(k^2-\omega_n^2)z^{-1} + (k^2+\omega_n^2-kQ)z^{-2}} \quad (9)$$

with *k* being $2/T_s$. To simplify, (9) is rewritten as

$$G_{notch}(z) = \frac{1}{2} \cdot \frac{(1+a_2) - 2a_1 z^{-1} + (1+a_2)z^{-2}}{1 - a_1 z^{-1} + a_2 z^{-2}} \quad (10)$$

in which a_1 and a_2 are the parameters of the notch filter, and they can be expressed as

$$a_1 = \frac{2(k^2-\omega_n^2)}{k^2+\omega_n^2+kQ}, \quad a_2 = \frac{k^2+\omega_n^2-kQ}{k^2+\omega_n^2+kQ} \quad (11)$$
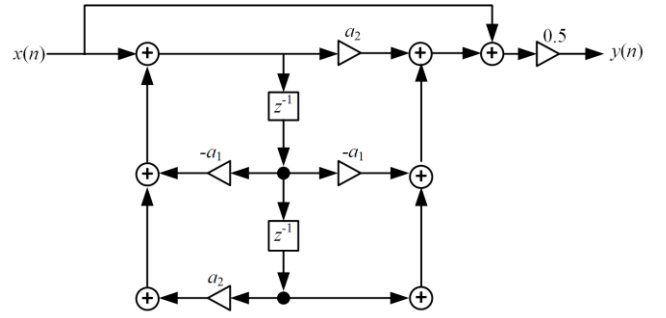

Fig. 4. Direct-Form II transposed (DFIIt) structure for the implementation of a digital notch filter.

It should be noted that the notch filter transfer-function given by (10) is characterized by the two parameters a_1 and a_2 as shown in (11). As a consequence, the notch filter $G_{notch}(z)$ can be conveniently implemented in a digital signal processor by using the Direct-Form II transposed (DFIIt) structure, as it is shown in Fig. 4. According to (9), the notch filter can be rewritten as

$$G_{notch}\left(e^{j\omega T_s}\right) = \frac{\cos\omega T_s\left(k^2+\omega_n^2\right) - \left(k^2-\omega_n^2\right)}{\cos\omega T_s\left(k^2+\omega_n^2\right) - \left(k^2-\omega_n^2\right) + jkQ\sin\omega T_s} \quad (12)$$

When the rejection bandwidth Ω and its minimum attenuation gain *x* are specified, the magnitude of (11) can be obtained by solving,

$$\left\{\left(k^2+\omega_n^2\right)\cos\omega T_s - \left(k^2-\omega_n^2\right)\right\}^2 \lambda^2 = k^2 Q^2 \sin^2\omega T_s \quad (13)$$

where λ can be expressed as

$$|\lambda| = \sqrt{10^{x/10} - 1} \quad (14)$$

Substituting $\omega = \omega_n \pm \Omega/2$ into (13) yields

$$\Omega T_s = \arccos\frac{\lambda^2\left(k^2+\omega_n^2\right)^2 - k^2 Q^2}{\lambda^2\left(k^2+\omega_n^2\right)^2 + k^2 Q^2} \quad (15)$$

which will result in the magnitude of (12) to be -*x* dB. Then, the two coefficients a_1 and a_2 of the notch filter can be calculated as,

$$a_1 = \frac{2\cos\omega_n T_s}{1+\lambda\cdot\tan\left(\Omega T_s/2\right)}, \quad a_2 = \frac{1-\lambda\cdot\tan\left(\Omega T_s/2\right)}{1+\lambda\cdot\tan\left(\Omega T_s/2\right)} \quad (16)$$

It is indicated in (14) and (16) that the constant parameters a_1 and a_2 are determined by the notch frequency ω_n, the desired rejection bandwidth Ω, and the minimum attenuation gain *x*. Moreover, the quality factor *Q* is absent in (16). Actually, the quality factor *Q* is replaced by

$$Q = \frac{\lambda}{k}\left(k^2 + \tan^2\left(\frac{\omega_n T_s}{2}\right)\right)\tan\left(\frac{\Omega T_s}{2}\right) \quad (17)$$

III. PARAMETER SENSITIVITY ANALYSIS OF THE CURRENT CONTROL LOOP WITH THE CONVENTIONAL DIGITAL NOTCH FILTER

In the following, the effectiveness of the conventional notch filter based active damping will be discussed considering the parameter drifting of the *LCL* filter. Here, it should be emphasized that there is a critical condition (i.e., $f_{res}=f_s/6$) dividing the entire frequency range into unstable and stable regions for both the ICF and GCF control [4]. Clearly, the notch filter
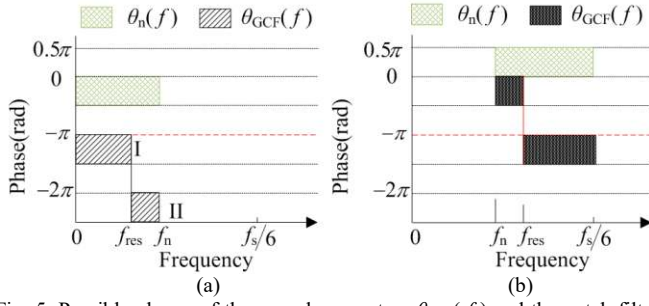
Fig. 5. Possible phases of the open-loop system $\theta_{\text{GCF}}(f)$ and the notch filter $\theta_n(f)$ considering different resonant frequencies of the *LCL* filter: (a) in case of $f_n > f_{\text{res}}$ and (b) in case of $f_n < f_{\text{res}}$.

TABLE II.
POSSIBLE PHASE LOCATION OF THE GCF CONTROL LOOP WITH DIFFERENT
RESONANT FREQUENCIES.

	$f_n > f_{\text{res}}$		$f_n < f_{\text{res}}$	
Freq. region	GCF I: $f_{\text{res}} \in (0, f_s/6)$		GCF I: $f_{\text{res}} \in (0, f_s/6)$	
$\theta_n(f)$	Phase Lag		Phase Lead	
	$f < f_{\text{res}}$	$f > f_{\text{res}}$	$f < f_{\text{res}}$	$f > f_{\text{res}}$
	I	II	III	IV
$\theta_{\text{GCF}}(f)$	$\left(-\dfrac{3}{2}\pi, -\pi\right)$	$\left(-\dfrac{5}{2}\pi, -2\pi\right)$	$\left(-\dfrac{1}{2}\pi, 0\right)$	$\left(-\dfrac{3}{2}\pi, -\pi\right)$
Stability	Stable		Unstable	

based active damping is to stabilize the current control loop, when the resonant frequency of the *LCL* filter locates in the unstable regions.

A. Active Damping using the GCF Control

According to [4] and Fig. 1(b), the unstable region for the GCF control (denoted as GCF I) is the frequency range of 0 to $f_s/6$, considering the sampling and computation process delay as T_s (i.e., $\delta = 1$). When the notch filter is adopted, the phase of the open-loop system will become

$$\theta_{\text{GCF}}(f) = \theta_{\text{delay}}(f) + \theta_{G_{i2}}(f) + \theta_n(f)$$

$$= \begin{cases} -\dfrac{\pi}{2} - 3\pi\dfrac{f}{f_s} + \theta_n, & f < f_{\text{res}} \\ -\dfrac{3\pi}{2} - 3\pi\dfrac{f}{f_s} + \theta_n, & f > f_{\text{res}} \end{cases} \quad (18)$$

with $\theta_{\text{GCF}}(f)$ being the phase of the open-loop system of the GCF control and $\theta_n(f)$ being the phase of the notch filter as a function of the frequency f. In the region of the GCF I, the notch frequency f_n is commonly placed at the resonant frequency f_{res} to damp the resonant peak of the *LCL* filter, as discussed in [22]. However, when the parameters of the *LCL* filter have a positive variation (e.g., 10% increases in the capacitor value), the resonant frequency f_{res} will drift from its nominal, and become smaller than the designed notch frequency f_n, affecting the damping performance. As the notch filter has a maximum of 90° phase lag that can be introduced to the open-loop system around the resonant frequency when $f_n > f_{\text{res}}$. By contrast, if the actual resonant frequency f_{res} becomes larger than the designed notch frequency f_n due to a negative parameter variation of the *LCL* filter, the notch filter then will present a maximum of 90° phase lead around the resonant frequency. According to (18), Table II summarizes the possible location
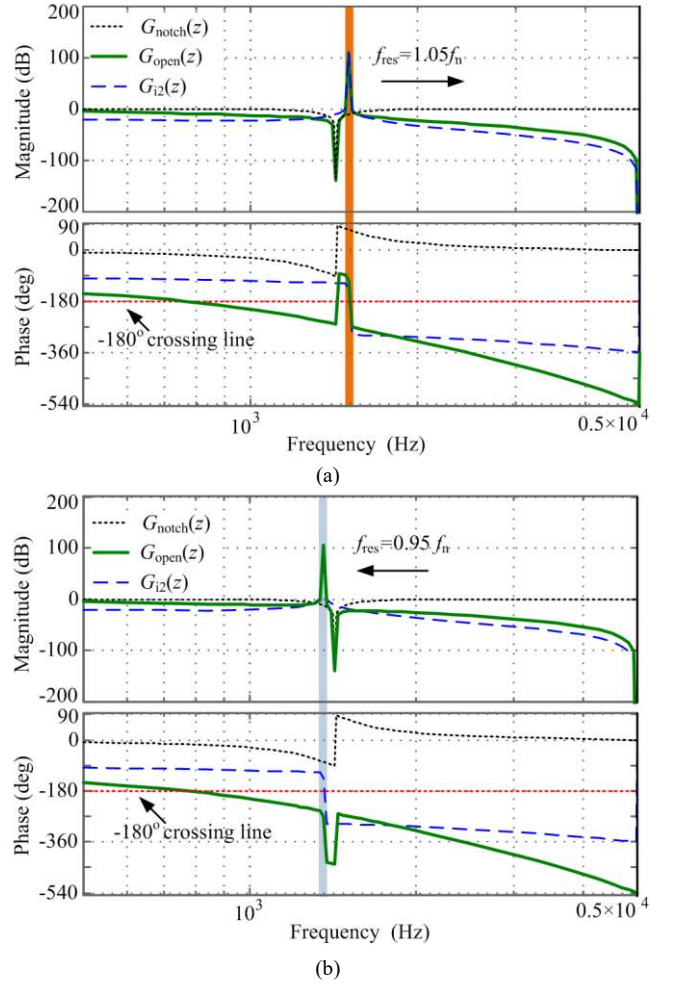

Fig. 6. Bode plot of open-loop with different resonant frequencies when the grid-side current is fed back to the control loop (i.e., GCF control): (a) C_f with -10% variation, f_{res}=1452 Hz, f_n=1377 Hz (i.e., $f_n < f_{\text{res}}$); and (b) C_f with +10% variation, f_{res}=1313 Hz, f_n=1377 Hz (i.e., $f_n > f_{\text{res}}$).

of the notch filter phase $\theta_n(f)$ and the resultant phase of the open-loop system $\theta_{\text{GCF}}(f)$, in the consideration of both negative and positive variations of the resonant frequencies f_{res} of the *LCL* filter.

To further illustrate the impact of resonance drifting on the damping performance, the phases of the notch filter $\theta_n(f)$ and the resultant open-loop system $\theta_{\text{GCF}}(f)$ are plotted in Fig. 5(a) and (b), respectively. Fig. 5(a) indicates that in the case of $f_n > f_{\text{res}}$, the phase of the notch filter (green zone) has a maximum of 90° phase-lag around the resonant frequency f_{res}. It thus can ensure the phase of the open-loop system $\theta_{\text{GCF}}(f)$ always smaller than $-\pi$, in return, implying that the system is stable. Additionally, Fig. 5(b) shows a different phenomenon where $f_n < f_{\text{res}}$ and the resultant phase of the open-loop system $\theta_{\text{GCF}}(f)$ is compensated by the notch filter (has a maximum of 90° phase-lead) to be larger than $-\pi$ before the resonance f_{res}. However, when $f > f_{\text{res}}$, $\theta_{\text{GCF}}(f)$ changes below $-\pi$, indicating a $-180°$-crossing around the resonant frequency. Hence, the system becomes unstable.

This is further confirmed by the Bode plots shown in Fig. 6, where $C_f = 14.1 \, \mu F$ with a decrease and increase of 10% in the capacitor value, respectively. As it is indicated in Fig. 6(a), due to the decrease in the capacitor value, $f_n < f_{\text{res}}$. As a result,

TABLE III.
POSSIBLE PHASE LOCATION OF THE ICF CONTROL LOOP WITH DIFFERENT RESONANT FREQUENCIES.

	$f_n > f_{res}$				$f_n < f_{res}$			
Freq. region	ICF II: $f_{res} \in (f_s/6, f_s/3)$		ICF III: $f_{res} \in (f_s/3, f_s/2)$		ICF II: $f_{res} \in (f_s/6, f_s/3)$		ICF III: $f_{res} \in (f_s/3, f_s/2)$	
θ_n	Phase Lag				Phase Lead			
	$f < f_{res}$ I	$f > f_{res}$ II	$f < f_{res}$ III	$f > f_{res}$ IV	$f < f_{res}$ V	$f > f_{res}$ VI	$f < f_{res}$ VII	$f > f_{res}$ VIII
$\theta_{ICF}(f)$	$\left(-\pi, -\frac{1}{2}\pi\right)$	$\left(-2\pi, -\frac{3}{2}\pi\right)$	$\left(-\frac{3}{2}\pi, -\pi\right)$	$\left(-\frac{5}{2}\pi, -2\pi\right)$	$\left(0, \frac{1}{2}\pi\right)$	$\left(-\pi, -\frac{1}{2}\pi\right)$	$\left(-\frac{1}{2}\pi, 0\right)$	$\left(-\frac{3}{2}\pi, -\pi\right)$
Stability	Unstable		Stable		Stable		Unstable	

even when the phase of the notch filter is positive at the actual resonant frequency, $\theta_n(f)$ is insufficient to compensate the phase of the open-loop system, leading to the -180°-crossing occurrence at the resonant frequency. Thus, the system is unstable. However, in the case of $f_n > f_{res}$, the phase of the notch filter is negative. It is observed that the phase lag of the notch filter is able to pull down the phase of the open-loop system, and thus at the resonant frequency, there is no occurrence of -180°-crossing, as it is highlighted in Fig. 6(b). As a consequence of the introduced phase lag, the system will be stable. Hence, the above indicates that in the region GCF I, introduce a proper phase lag help to stabilizing the current control loop.

B. Active Damping using the ICF Control

Similarly, the sensitivity analysis of the notch filter based active damping for the ICF control is carried in the unstable region (i.e., the resonant frequency locates within $f_s/6$ to $f_s/2$). When the notch filter is employed in current control loop, the phase of the open-loop system (denoted as $\theta_{ICF}(f)$) will become

$$\theta_{ICF}(f) = \theta_{delay}(f) + \theta_{G_{i1}}(f) + \theta_n(f)$$

$$= \begin{cases} -\dfrac{\pi}{2} - 3\pi\dfrac{f}{f_s} + \theta_n, & f < f_0 \\[2mm] \dfrac{\pi}{2} - 3\pi\dfrac{f}{f_s} + \theta_n, & f < f_{res} \\[2mm] -\dfrac{\pi}{2} - 3\pi\dfrac{f}{f_s} + \theta_n, & f > f_{res} \end{cases} \quad (19)$$

According to Fig. 3, the phase of the notch filter $\theta_n(f)$ varies from -90° to +90° before the Nyquist frequency, and this 180°phase change occurs at the notch frequency. Hence, assuming that the resonant frequency f_{res} is slightly drifted away from its initial setting ($f_{res} = f_n$), the notch filter phase $\theta_n(f)$ may introduce -90° or +90° phase at the resonant frequency f_{res}. As a consequence, the phase of the open-loop system $\theta_{ICF}(f)$ around the notch filter frequency can be expressed as

$$\theta_{ICF}(f)\Big|_{f_n < f_{res}, \theta_n = \frac{\pi}{2}} = \begin{cases} \pi - 3\pi\dfrac{f}{f_s}, & f < f_{res} \\[2mm] -3\pi\dfrac{f}{f_s}, & f > f_{res} \end{cases} \quad (20a)$$

when $f_n < f_{res}$, and

$$\theta_{ICF}(f)\Big|_{f_n > f_{res}, \theta_n = -\frac{\pi}{2}} = \begin{cases} -3\pi\dfrac{f}{f_s}, & f < f_{res} \\[2mm] -\pi - 3\pi\dfrac{f}{f_s}, & f > f_{res} \end{cases} \quad (20b)$$

when $f_n > f_{res}$.

Eq. (20) implies that when the resonant frequency f_{res} locates at $f_s/3$, the resultant phase $\theta_{ICF}(f)$ may be equal to –180° at the resonant frequency in both cases, and inevitably leading to –180°-crossing around the resonant peak. However, when the resonant frequency f_{res} locates in $(f_s/6, f_s/3)$, it is shown in (20a) that the –180°-crossing will not occur at the resonant frequency f_{res}; while, there will be –180°-crossing at the resonant frequency f_{res} as it is indicated in (20b). Furthermore, when the resonant frequency f_{res} locates in $(f_s/3, f_s/2)$, Eq. (20a) implies that –180°-crossing at the resonant frequency f_{res} cannot be avoided. Hence, it suggests that the unstable region of the ICF control can be further divided into two parts as ICF II ($f_{res} \in (f_s/6, f_s/3)$) and ICF III ($f_{res} \in (f_s/3, f_s/2)$). Assuming that the parameters of the *LCL* filter have a positive variation (e.g., 10% increases in the capacitor value), the resonant frequency of the *LCL* filter f_{res} will become smaller than the designed notch frequency f_n (i.e., $f_n > f_{res}$). In that case, the notch filter has a maximum of 90° phase-lag around the resonant frequency f_{res}. However, a parameter decrease in the *LCL* filter will result in a larger resonant frequency ($f_n < f_{res}$). In that case, the notch filter has a maximum of 90° phase-lead around the resonant frequency f_{res}, when $f_n < f_{res}$. Accordingly Table III gives the resultant phase $\theta_{ICF}(f)$ of the open-loop system with negative and positive variations in the resonant frequency.

The phases of the open-loop system and the corresponding phase of the notch filter are further plotted in Fig. 7. It can be observed in Fig. 7(a) and (b) that the phase of the notch filter $\theta_n(f)$ has a 90°-phase-lag around the resonant frequency f_{res} (i.e. $f_n > f_{res}$). Hence, in the region of ICF II, the phase of the open-loop system will be larger than $-\pi$ before the resonant frequency f_{res}, However, in the region of ICF III, the resultant phase of the open loop system $\theta_{ICF}(f)$ will become smaller than $-\pi$, as shown in Fig. 7(b). When $f > f_{res}$, the phase of the open-loop system goes below $-\pi$ in both regions of ICF II and ICF III, as shown in Fig. 7(a) and (b). This implies that a –180°-crossing is inevitable in the region of ICF II due to the phase lag of the notch filter, resulting in an unstable control system. Fortunately, the phase lag of the notch filter can contribute to stabilizing the control loop in the region of ICF III, since the phase of the open-loop system $\theta_{ICF}(f)$ with the notch filter is already below –180° before the resonant frequency f_{res} (see Fig. 7(b)). This phenomenon is confirmed in the Bode plots shown in Fig. 8(a) and (b), where $G_{i1}(z)$, $G_{open}(z)$ and $G_{notch}(z)$ are corresponding given in Eqs. (1a), (7) and (9) and $C_f = 4.7$ μF and 1.5 μF with a variation of +10% in the capacitance, respectively. As it can be seen in Fig. 8(a), in the region of ICF II, the notch filter will lose the ability to cancel out the resonant peak of the *LCL* filter (i.e., $f_{res} = 0.95f_n = 2266$ Hz),
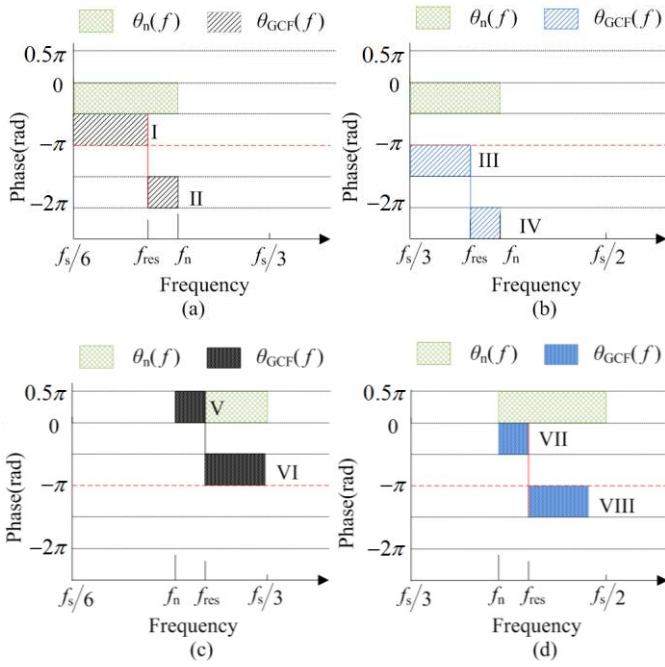
Fig. 7. Possible phases of the open-loop system $\theta_{ICF}(f)$ and the notch filter $\theta_n(f)$ considering different resonant frequencies of the LCL filter using ICF control: (a) region ICF II: in case of $f_n > f_{res}$; (b) region ICF III: in case of $f_n > f_{res}$; (c) region ICF II: in case of $f_n < f_{res}$; (d) region ICF III: in case of $f_n < f_{res}$.

leading to instability. On the contrary, Fig. 8(b) shows that the phase lag of the notch filter can pull down the phase of the open-loop system in the region of ICF III, and prevent it from crossing the −180°-line at the resonant frequency (i.e., $f_{res} = 0.95f_n = 4011$ Hz). It means that the system remains stable even when the resonant peak of the LCL filter is not mitigated, as illustrated in Fig. 8(b).

A different result is obtained in the case of a negative parameter variation in the LCL filter (e.g, 10% decreases in the capacitor value), where $f_n < f_{res}$ and the phase of the notch filter $\theta_n(f)$ has a maximum of 90°-lead around the resonant frequency f_{res}. Hence, according (18) and Table III, the phase of the open-loop system will be larger than −180° between f_n and $f_s/3$ in the region of ICF II, as shown in Fig. 7(c) and demonstrated in Fig. 8(c). That is to say, the notch filter will prevent the entire open-loop system from crossing the −180°-line and thus the current control loop will be stable. However, in the region of ICF III, the phase lead (i.e., $\theta_n(f)$) provided by the notch filter is insufficient to compensate the phase of the open-loop system $\theta_{ICF}(f)$ after the resonant frequency, as shown in Fig. 7(d). Consequently, the phase of the open-loop system will cross the −180°-line, leading to an unstable control loop, which is also verified in Fig. 8(d). From Table III and Fig. 8, it can be concluded that the phase lead of the notch filter can maintain the stability of the current control system in the region of ICF II; while for the region of ICF III, the stability may lose due to the −180°-crossing of the open-loop system around the resonant frequency f_{res}. To sum up, Fig. 5 to Fig. 8 show how the notch filter based active damping is affected by the LCL filter parameter variations. However, it should be noted that, when the resonant frequency drifts too far from the designed notch frequency (i.e., the nominal resonant frequency), the phase of the notch filter will become in-

sufficient to provide either a phase lag or lead to prevent the open-loop system from crossing the −180°-line around the resonant frequency. This can be illustrated and further summarized by means of the pole-and-zero plots of the closed-loop system given as

$$G_{close}(z) = \frac{G_{open}(z)}{1 + G_{open}(z)} \qquad (21)$$

where $G_{close}(z)$ is the transfer-function of the closed-loop system. It can be seen in pole-and-zero plots of Fig. 9 that, when the resonant frequency f_{res} is equal to the notch frequency (i.e., $f_n = f_{res}$), the unstable pole of the LCL filter will be canceled out by the zero of the notch filter, and thus the system stability is ensured as discussed above. However, parameter drifting makes $f_n \neq f_{res}$, in the region of ICF II (see Fig. 9(b)), the decrease in the resonant frequency will force the unstable pole away from the zeros of the notch filter and thus out of the unity circle, challenging the entire system stability. In contrast, increasing the resonant frequency will move the unstable poles into the unit circle, resulting in a stable system, as shown in Fig. 9(b). Nevertheless, Fig. 9(b) also indicates that if the capacitance drifts too far from its nominal value, the poles will go out of the unit circle again, and thus the entire system goes to be unstable; if the resonant frequency locates in the regions of GCF I and ICF III, the situation is much different, as shown in Fig. 9(a) and (c). Fig. 9(c) demonstrates that the resonant pole will move out of the unit circle if the positive resonant frequency variation is too large, and thus the system becomes unstable again. In contrast, Fig. 9(a) shows that even with a 50% increase in the capacitance, the pole remains inside the unit circle. This is due to the phase lag of the notch filter still can pull down the phase of the open loop system to cross -180°-line before the resonant frequency, indicating a stable current control system.

IV. PROPOSED DIGITAL NOTCH FILTER DESIGN FOR ROBUST ACTIVE DAMPING

As summarized in Table III, the phase lead or lag of the notch filter can contribute to the stability of the current control loop in particular areas depending on which current is fed back for the control (i.e., ICF or GCF). Hence, by using a phase adjustor to introduce phase lead or lag may help to improve control loop stability. The phase adjustor can be a digital filter (high-pass, low-pass, and all-pass), lead-lag network or notch filter. The high pass filter can only provide phase lead with maximum 90 degree, and it may amplify the high frequency noise. By contrast, the low-pass type can avoid high frequency noise, but it only introduce maximum 90 degree phase lag. Using an all-pass filter can introduce more phase lag than low-pass type, but unfortunately, its phase calculation is complicate. Similar drawback can be found in using lead-lag network, which has identified in [15] that it can provide phase lead or lag around particular frequency. In additional, the magnitude of lead-lag network is non-zero, which may significant move the desired crossover frequency of current control loop. Start from this, the notch filter is much prior than the former mentioned due to its magnitude is smaller than 0 dB in the whole frequency range and can provide phase lag or lead. Thus, with continue the sensitive analysis done in § III,
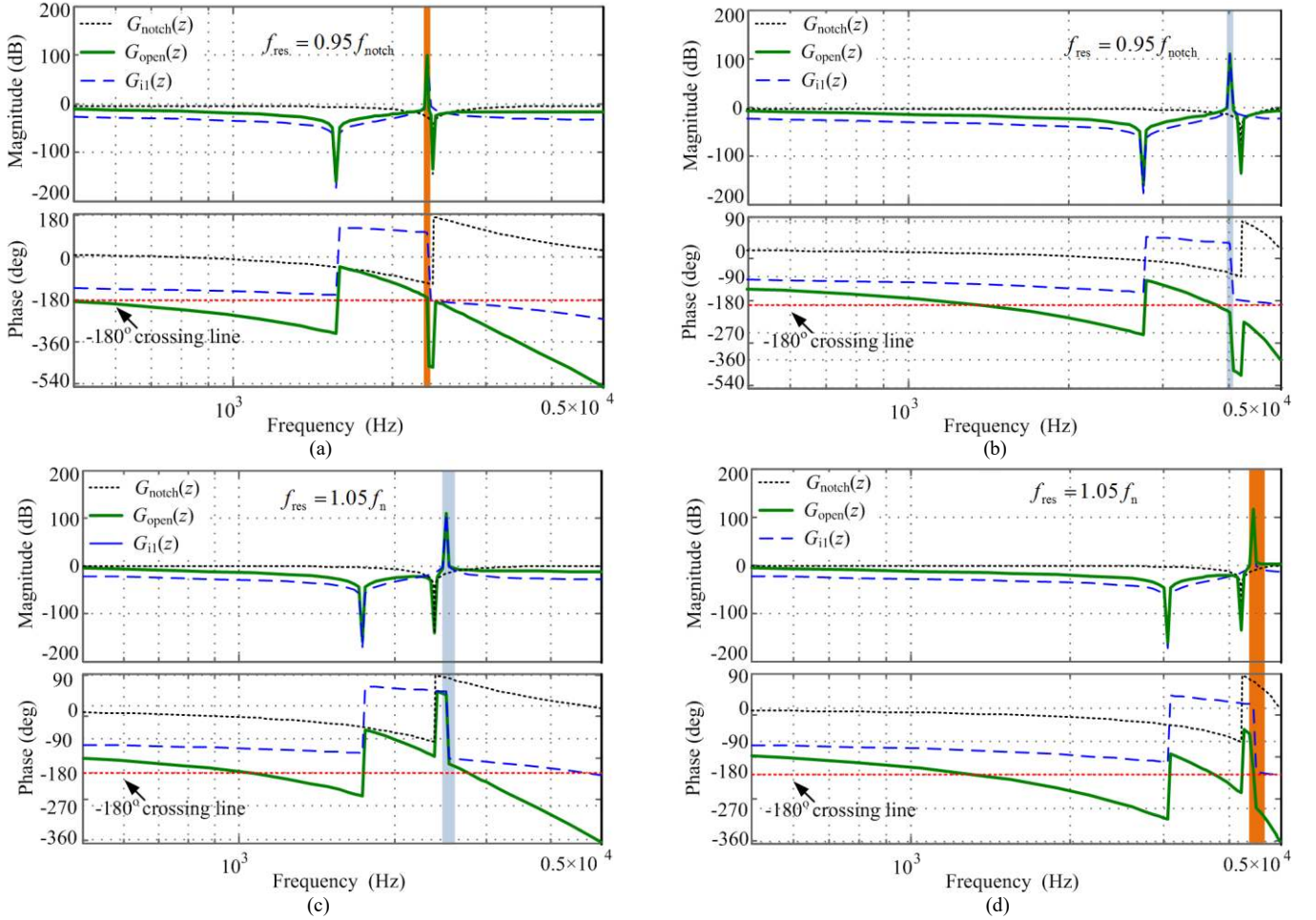
Fig. 8. Bode plots of the open-loop system with different resonant frequencies in case of ICF control: (a) ICF II: $C_f = 4.7$ μF with a +10% variation of capacitance, $f_n > f_{res}$, $f_n = 2385$ Hz; (b) ICF III: $C_f = 1.5$ μF with +10% variation of capacitance, $f_n > f_{res}$ and $f_n = 4222$ Hz; (c) ICF II: $C_f = 4.7$ μF with -10% variation of, $f_n < f_{res}$ and $f_n = 2385$ Hz; (d) ICF III: $C_f = 1.5$ μF with -10% variation of capacitance, $f_n < f_{res}$ and $f_n = 4222$ Hz.
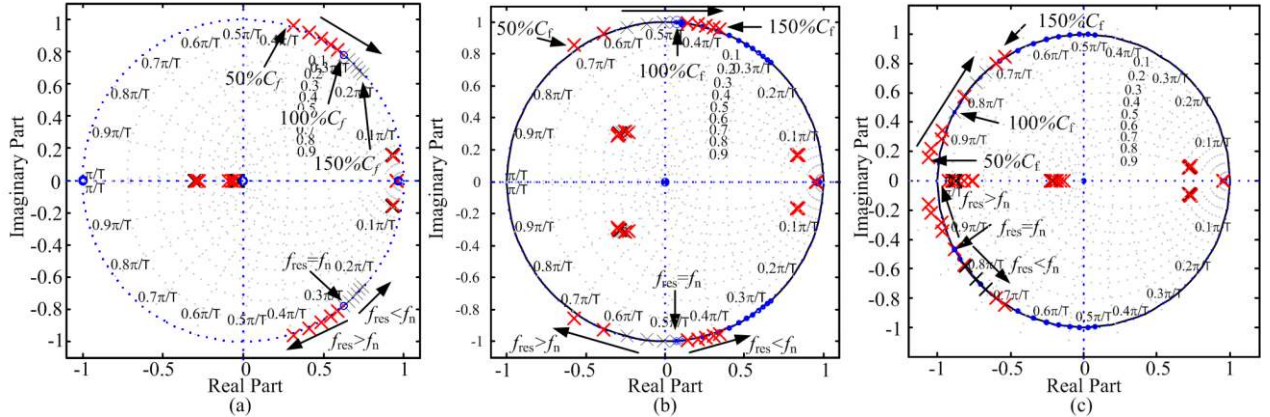

Fig. 9. Pole and zero maps of the closed-loop current control loop with different resonant frequencies due to the *LCL* filter capacitance with ± 50% variation: (a) region GCF I; (b) region ICF II, and (c) region ICF III.

the notch filter is employed here adjust the phase of current control loop. In contrast to the conventional method [21], in the following proposed design, the notch frequency is placed away from the resonant frequency so that it can provide sufficient phase lead or lag around the resonant frequency f_{res}. That is to say, the frequency of the notch filter will not be exactly located at but determined by the resonant frequency f_{res} of the *LCL* filter (i.e., the delay-demanded areas). Nevertheless, the

major objective is to ensure that there is no − 180°-crossing at the resonant frequency, guaranteeing the stability of the current control loop. Since the notch filter presents phase-lead or phase-lag characteristics in difference frequency ranges, which is utilized in the proposed method as a phase adjustor to modify the phase characteristic of the current control loop accordingly. Notably, the PI controller (see Fig. 2) should also be designed carefully [3].

A. Proposed Design of the Digital Notch Filter for Robust Active Damping using the ICF Control

As aforementioned, the region of the ICF II is identified as a compensation-demanded region – the time delay induced in the digital control system needs to be compensated in such a way to stabilize the entire current control. In order to make the controller more robust against the grid impedance and *LCL* filter parameter variations, the notch frequency is designed by placing the notch frequency below the nominal resonant frequency of the *LCL* filter, which can contribute to an increased stability margin for the region of ICF II. Normally, low voltage power transformers and long distribution transmission wires will introduce a large set of grid impedance (around 0.1 mH [31], [33]), and this grid impedance will be further enlarged if a number of inverters are connected in parallel [33]. Hence, a very weak grid with $L_g = 10$ mH is selected in this paper. This also indirectly enables the robustness verification of the proposal. In order to achieve that the current control loop is stable even in such a weak grid (e.g., $L_g = 10$ mH), the maximum notch frequency ω_n is calculated according to (2) when $L_g = 10$ mH. Thus, when $f_{res} > f_n$, the phase lead introduced by the notch filter around the resonant frequency can compensate the time delay in the entire control system, as demonstrated in Fig. 10, where the Bode plot of the open loop without the notch filter based active damping is also presented.

It can be observed in Fig. 10 that, the phase of the open-loop system (green dashed-line) without the active damping will cross the $-180°$-line at the resonant frequency. In contrast, when the notch filter is incorporated, the phase lead of the notch filter will help the open-loop system cross the $-180°$-line beyond the resonant frequency f_{res}, resulting in a stable system. Also, as indicated in Fig. 10, there are three crossover frequencies: ω_{c1}, ω_{c2}, and ω_{c3} ($\omega_{c1} < \omega_{res}$, $\omega_o < \omega_{c2} < \omega_{res}$, $\omega_{c3} > \omega_{res}$) to be designed. It is apparent that the phase margins of φ_3 at ω_{c3} are smaller than φ_1 and φ_2 at ω_{c1} and ω_{c2}, respectively. Hence, in order to ensure the control performance, the phase margins of φ_3 should be larger than a specified value φ.

The phase of the notch filter can be derived from (12) as,

$$\theta_n(\omega) = -\arctan \frac{\lambda \tan \frac{\Omega T_s}{2} \sin \omega T_s}{\cos \omega_n T_s - \sin \omega T_s} \tag{22}$$

indicating that the phase of the notch filter at the resonant frequency ω_{res} is positive (since $\omega_{res} > \omega_n$), which thus can be employed to compensate the phase lag of the entire current control system at the resonant frequency, as shown in Fig. 10. Since the magnitude and the phase contributions of the *LCL* filter become small at the crossover frequency ω_{c1}, the response of the *LCL* filter will be dominated by the total series inductance [3]. In addition, the PI controller also makes little phase contribution at the crossover frequencies ω_{c1}, i.e., $\angle G_{pi}(e^{j\omega_{c1}T_s}) \approx 0$. It is thus reasonable to approximate the *LCL* filter as a single *L* filter ($L = L_1 + L_2$) in a low frequency range [6]. Consequently, considering $\delta = 1$, the open-loop current control system (8) can be simplified as [4]

$$G_{open}(z) = z^{-1} \cdot G_{pi}(z) \cdot V_{dc} \cdot G_{notch}(z) \cdot \frac{T_s}{(z-1)(L_1+L_2)} \tag{23}$$

Moreover, in the frequency range of $\omega > \omega_{res}$, the phase behavior of the *LCL* filter can also be approximated as a single *L*

filter ($L = L_1 + L_2$), as discussed in [4]. Hence, the phase margin of φ_3 can be derived from (22) and (23) as

$$\begin{aligned}\varphi_3 &= \pi + \angle G_{i1}(z) + \angle G_{pi}(z) + \angle z^{-1} + \angle G_{notch}(z) \\ &= \pi - \frac{\pi}{2} - \frac{3}{2}\omega T_s + \theta_n(\omega) \\ &\geq \varphi\end{aligned} \tag{24}$$

Hence, for a given phase margin φ, the rejection bandwidth Ω of the notch filter can be obtained.

In order to tune the PI controller, the crossover frequency ω_{c1} should be derived. Since the crossover frequency ω_{c1} is much smaller than the *LCL* filter resonant frequency ω_{res}, the gain of the notch filter is almost flat at the crossover frequency ω_{c1}, as it is shown in Fig. 10. Thus, the notch filter has a negligible impact on the crossover frequency location of the entire current control loop. It means that the crossover frequency ω_{c1} of the current control system with the notch filter can be approximated to the one when the notch filter is absent in the current control loop. Hence, according to the discussions in [3], the proportional gain should ensure enough phase margin φ_m, e.g., $\varphi_m = 60°$ for the undamped open loop system given by

$$G_{open}(z) = z^{-1} \cdot G_{pi}(z) \cdot V_{dc} \cdot \frac{T_s}{(z-1)(L_1+L_2)} \tag{25}$$

Thus, the crossover frequency is calculated as [3]

$$\omega_{c1} = \frac{\pi}{9T_s} \tag{26}$$

Then, the phase margin of φ_1 for the open-loop system with the active damping can be calculated from the difference between φ_m and the phase of the notch filter $\theta_n(\omega_{c1})$ (i.e., $\varphi_1 = 180 + \varphi_m + \theta_n(\omega_{c1})$). Taking $\varphi_3 = \varphi = \pi/9$ (i.e., 20°) for an example, the -3 dB ($x = 3$, $\lambda = 1$, according to (15)) rejection bandwidth Ω can be calculated from (22). In that case, the rejection bandwidth Ω will be around $2\pi \times 2500$ rad/s, and the resultant phase margin of φ_1 at the crossover frequency ω_{c1} is around 39°.

For the region of ICF III, a phase lag is required to stabilize the current control system, where the design of the notch filter
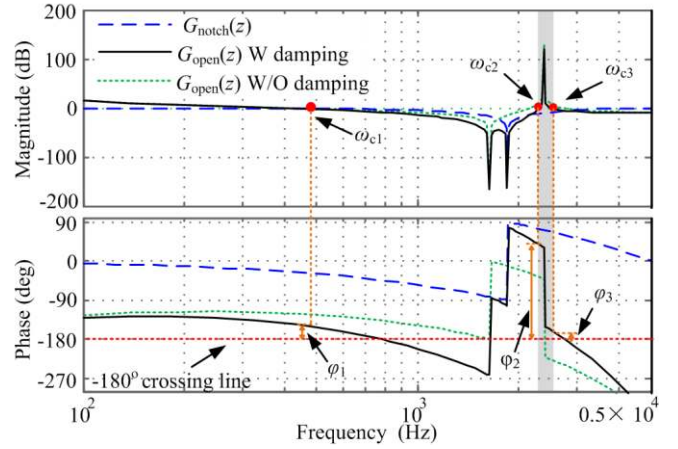

Fig. 10. Bode plots of the open-loop current control system (with and without the notch filter based active damping): the notch frequency f_n is placed below the nominal resonant frequency of the *LCL* filter for the region of ICF II (i.e., $f_{res} \in (f_s/6, f_s/3)$).

Fig. 11. Bode plot of the open-loop current control system (with and without the dual notch filters based active damping), where f_n is placed larger than the resonant frequency f_{res} for the region of ICF III (i.e., $f_{res} \in (f_s/3, f_s/2)$).
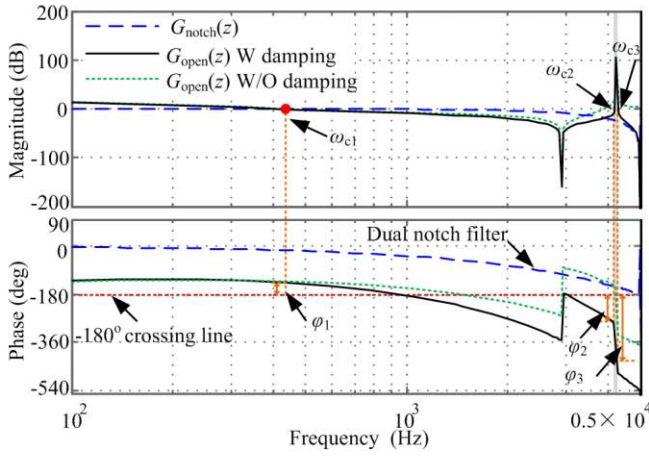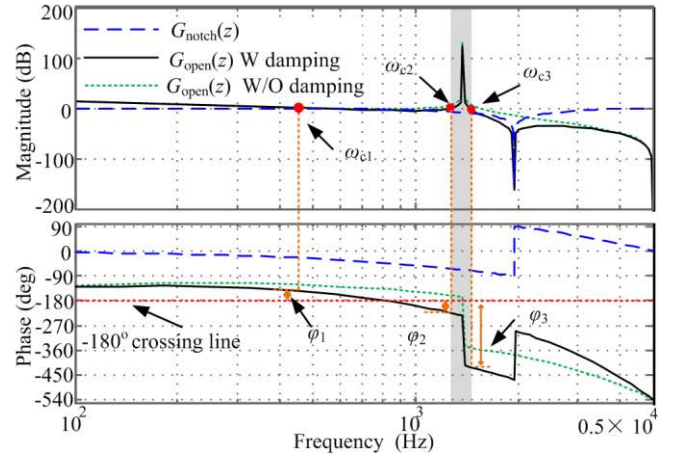

Fig. 12. Bode plot of the open-loop current control system (with and without the notch filter based active damping), where f_n is placed larger than the resonant frequency f_{res} for the region GCF I (i.e., $f_{res} \in (0, f_s/6)$).

is more complicated compared to that demonstrated above. That is because the notch frequency has to be much beyond the resonant frequency in order to tolerate the impact of the filter parameter drifting on the stability. Considering a -50% change in the capacitance of the *LCL* filter, the notch frequency may have to locate beyond the Nyquist frequency according to the above analysis (§ III), which will degrade the performance of the notch filter. Alternatively, the notch frequency may be located exactly at the Nyquist frequency, and then the notch filter will present a purely phase-lag characteristic in the entire frequency range of below the Nyquist frequency, as shown in Fig. 11. However, if the notch frequency is very far away from the resonant frequency (e.g., when the notch frequency is placed at the Nyquist frequency), the phase lag of the notch filter will be insufficient to pull the phase of the open-loop system above -180° before the resonant frequency. In that case, two notch filters with the notch frequency designed exactly at the Nyquist frequency can be employed in order to introduce more phase-lag (maximum of 180° phase delay).

Fig. 11 illustrates the frequency responses of the open-loop system with two notch filters based active damping. It can be observed that there are three crossover frequencies: ω_{c1}, ω_{c2}, and ω_{c3} ($\omega_{c1} < \omega_{c2} < \omega_{res}$, $\omega_{c3} > \omega_{res}$), indicating that the phase margin of φ_1 at the crossover frequency ω_{c1} is the smallest one. Hence, similar to the region of ICF II, the phase margin of φ_1 should be larger than a specified value φ. In that case, the phase margin of φ_1 can be calculated as [4]

$$
\begin{aligned}
\varphi_1 &= \pi + \angle G_{i1}(z) + \angle G_{PI}(z) + \angle z^{-1} + \angle G_{notch}(z) + \angle G_{notch}(z) \\
&= \pi - \frac{\pi}{2} - \frac{3}{2}\omega T_s + 2\theta_n(\omega) \\
&\geq \varphi
\end{aligned}
$$

(27)

As a result, for a given phase margin φ, the -3 dB ($x = 3$, $\lambda = 1$, referring to (15)) rejection bandwidth Ω of the notch filter can be obtained. Taking $\varphi = \pi/4$ (i.e., 45°) for instance, the rejection bandwidth Ω calculated from (22) gives around $2\pi \times 2500$ rad/s, and the phase margin of φ_1 at the crossover frequency ω_{c1} will be around 47°, implying stable control systems.

B. Proposed Design of the Digital Notch Filter for Robust Active Damping using the GCF Control

As mentioned previously, the region of GCF I is identified as delay-demanded region and the resonant frequency maybe affected by the grid impedance. Fortunately, this impact does not bring side-effects on the stability of the GCF control, as it has been concluded in § III.A. However, the negative variations of the *LCL* filter parameters impose more impacts on the stability. Hence, the notch frequency should be designed higher than the resonant frequency so that a phase lag is introduced at the resonant frequency to make the system stable. For instance, assuming that the capacitor of the *LCL* filter decreases by 50% (i.e., $C_f = 14.1\ \mu F$), the maximum notch frequency ω_n can be calculated according to (2) and the Bode plot of the current open-loop system is then shown in Fig. 12. It can be seen that there are three crossover frequencies: ω_{c1}, ω_{c2}, and ω_{c3} ($\omega_{c1} < \omega_{c2} < \omega_{res}$, $\omega_{c3} > \omega_{res}$), among which the phase margin of φ_2 at ω_{c2} is the smallest one. Hence, similar to the ICF control, the phase margin of φ_2 should be larger than a specified value φ. When replacing φ_3 by φ_2, the phase margin of φ_2 can be calculated according to (24), where the rejection bandwidth Ω of the notch filter can be derived if a phase margin is specified as φ. Taking $\varphi = \pi/6$ rad (i.e., 30°) for an example, the -3 dB ($x = 3$, $\lambda = 1$, according to (15)) rejection bandwidth Ω from (22) gives around $2\pi \times 1600$ rad/s, which results in that the phase margin of φ_1 at the crossover frequency ω_{c1} will be around 55°, implying a stable control systems.

C. Parameter Sensitivity Analysis of the Closed-Loop System Stability in the z-Domain

Fig. 13 shows the root loci of the overall closed-loop current control system of (21), when the parameters of the *LCL* filter and also the grid impedance are varying. Fig. 13(a) to (c) are the cases when the ICF control is adopted with the resonant frequency in the region of ICF II; Fig. 13(d) to (f) are for the ICF control in the region of ICF III; and Fig. 13(g) to (i) are for the GCF control. In all cases, the proposed design has been employed.

As it can be seen in Fig. 13(a), although the grid impedance L_g varies from 0 mH (i.e., a very strong grid) to 10 mH (i.e., a very weak grid), the system is always stable. Fig. 13(b) and (c)
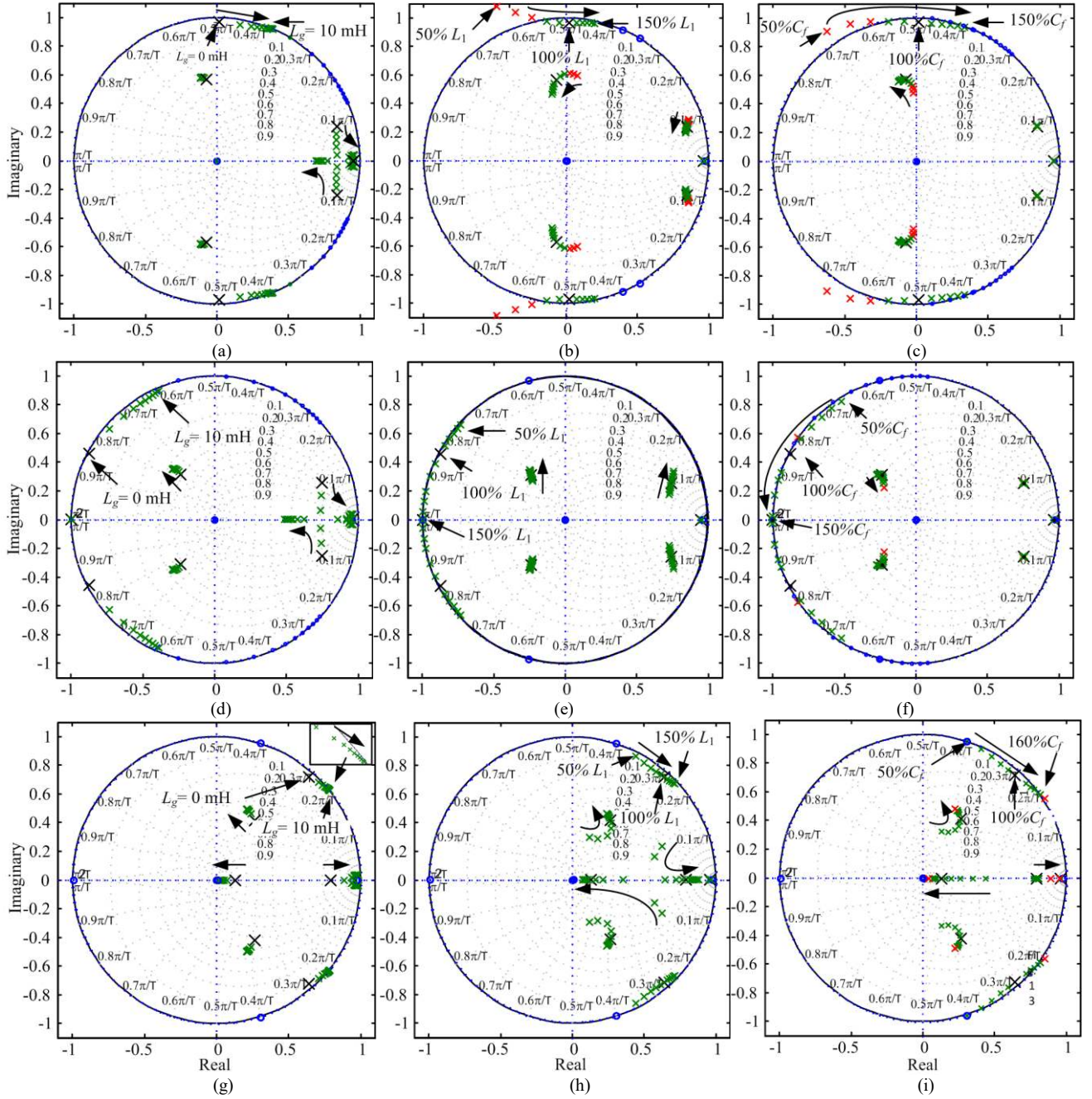
Fig. 13. Pole and zero location of the closed-loop control system when the grid impedance and the *LCL* filter parameter are varying: (a)~(c) for the ICF control with the resonant frequency in the region of ICF II; (d)~(f) for the ICF control with the resonant frequency in the region of ICF III; (g)~(i) for the GCF control in the region of GCF I: (a), (d), (g) grid impedance L_g varying from 0 mH to 10 mH; (b), (e), (h) inverter side inductor L_1 varying from 50% to 150% of the rated value; and (c), (f), (i) filter capacitor C_f varying from 50% to 150% of the rated.

show the stable ranges of the control system in the case of a varying inverter-side inductor L_1 and filter capacitor C_f of the *LCL* filter (from 50% to 150% of the rated value shown in Table I), respectively. It can be observed in Fig. 13(b) that for large variations of L_1, the current control system is stable, while instability occurs when $L_1 < 1.35$ mH (i.e., 75% of the rated value). Similarly, it can be seen in Fig. 13(c) that the current control system is stable in the case that $C_f > 3.52$ μF (i.e., 75% of the rated value). However, when the capacitance decreases further, the current control system becomes unstable, as shown in Fig. 13(c). This is because that in order to tolerate a wide range of grid impedance variations (e.g., up to 10 mH),

the notch frequency should be much lower than the resonant frequency. Thus, the phase lead of the notch filter will be very small at higher frequencies. However, the capacitance decreases will result in an increase of the resonant frequency of the *LCL* filter, where the phase lead of the notch filter cannot prevent the open-loop system from -180°-crossing at the resonant frequency, leading to instability.

The zero and pole plots of Fig. 13(d) to (f) show that the ICF control in the regions of ICF III and GCF I are much robust against both the grid impedance and *LCL* parameter variations. When the grid impedance L_g varies from 0 mH to 10 mH, the current control system is always kept stable. For the

TABLE IV.
PARAMETERS OF THE NOTCH FILTER FOR SIMULATIONS AND EXPERIMENTS.

Capacitance C_f	Resonant Frequency f_{res}	Current Feedback	Notch Filter Frequency f_n	Bandwidth of Notch filter Ω
1.5 μF	4222 Hz	ICF	5000 Hz	$2\pi\times2500$ rad/s
4.7 μF	2835 Hz	ICF	1855 Hz	$2\pi\times2500$ rad/s
14.1 μF	1377 Hz	GCF	1947 Hz	$2\pi\times1600$ rad/s

ICF control (in the region of ICF III), the current control system becomes unstable when the filter capacitance has a -50% variation, since the resonant frequency is drifted beyond the Nyquist frequency. For the GCF control, despite of the variations of the *LCL* parameters, the notch filter can guarantee the stability of the current control loop, since it has been considered during the design phase of the notch filter, which covers a ±50% variation of the capacitance or the inductance of the *LCL* filter. However, if the variations are much larger (e.g., 160% of the rated C_f), the current control loop will become unstable as the poles will go outside of the unit circle. This is due to that the phase lag of the notch filter is insufficient to "push" the phase of the open-loop system down below -180°-line at the crossover frequency ω_{c2}.

V. SIMULATION AND EXPERIMENTAL RESULTS

Referring to Fig. 1 and Fig. 2, simulations and experiments have been performed to verify the effectiveness of the proposed digital notch filter based active damping. The system parameters are given in Table I, where different values of capacitor are used in such a way to place the resonant frequency of the *LCL* filter in difference areas, as also summarized in Table IV. The simulations can be considered as a worse case, since the internal resistance of the inductors is neglected for simplicity. In the experiments, a 2.2-kW three-phase commercial inverter is connected to a 230-V/50-Hz grid through an isolation transformer, whose total leakage inductance of 2 mH formed the grid-side inductor (L_2) of the *LCL* filters. The inverter-side inductor L_1 is, on the other hand, designed according to the peak-to-peak current ripple ΔI_{Lx} of 40% of the rated current [33], resulting in $L_1 = 1.4$ mH, which is chosen as 1.8 mH in the laboratory setups due to the availability. By doing so, the ratio of L_2/L_1 is around 1.1, leading to that the peak-to-peak current ripple will be further reduced to below 2% of the rated current [35]. The control systems were implemented in a dSPACE DS 1103 system, and the notch filter parameters are given in Table IV.

Fig. 14 shows the simulation results of the proposed digital notch filter based active damping in the case of the ICF control and the GCF control. It can be seen in Fig. 14 that the current control system can operate stably, when the active damping is enabled. This confirms that the proposed digital notch filter based active damping can effectively ensure the system stability – the damping is achieved by the designed notch filter. In order to verify the effectiveness of the notch filter based active damping experimentally, the capacitance C_f of the *LCL* filter and the notch frequency f_n are selected as shown in Table IV. Hence, active damping is required for each case. Fig. 15 shows that the resonance in the case of either the ICF control or the GCF control is effectively damped, when the proposed digital notch filter based active damping is activated. However,
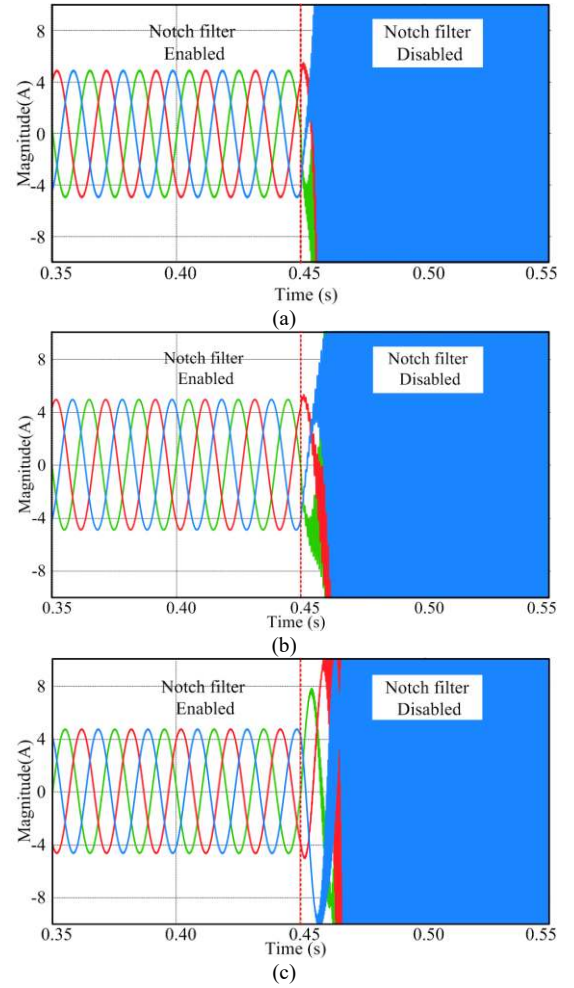

Fig. 14. Simulation results of the proposed digital notch filter based active damping for a three-phase grid-connected inverter system, where the active damping is disabled at $t = 0.45$ s for comparisons: (a) using the ICF control with the resonant frequency f_{res} =2385 Hz, i.e., in the region of ICF II, (b) using the ICF control with the resonant frequency f_{res} =4222 Hz, i.e., in the region of ICF III, and (c) using the GCF control with the resonant frequency f_{res} =1377 Hz, i.e., in the region of GCF I.

when the active damping is disabled, the resonance appears again and the system becomes unstable, as it is shown in Fig. 15. It is clear that an active damping is necessary for the current control system to maintain the stability and also the current quality. Those can be achieved when the proposed method is adopted, as verified by the experimental tests presented in Fig. 15. To further test the robustness of the proposed active damping in case of ICF control, an additional inductor of 1.8 mH is thus inserted between the grid and the grid side inductor L_2. Fig. 16 (a) and (b) show the test result of the three-phase system with different resonant frequencies. In these tests, when the notch filter is disabled, the controller is unable to stabilize the current control loop, and thus the grid currents start oscillating, as shown in Fig. 16 (a) and (b). In contrast, when the designed notch filter is enabled, the system resonance is effectively damped by the digital notch filter, and the system goes back to stable operation. For the case of the GCF control, the robustness test is done under a condition where the capacitance of the *LCL* filter is decreased to 9.4 μF, and the test results are presented in Fig. 16 (c). The reason for setting up this test condition is that the GCF control is much robust to
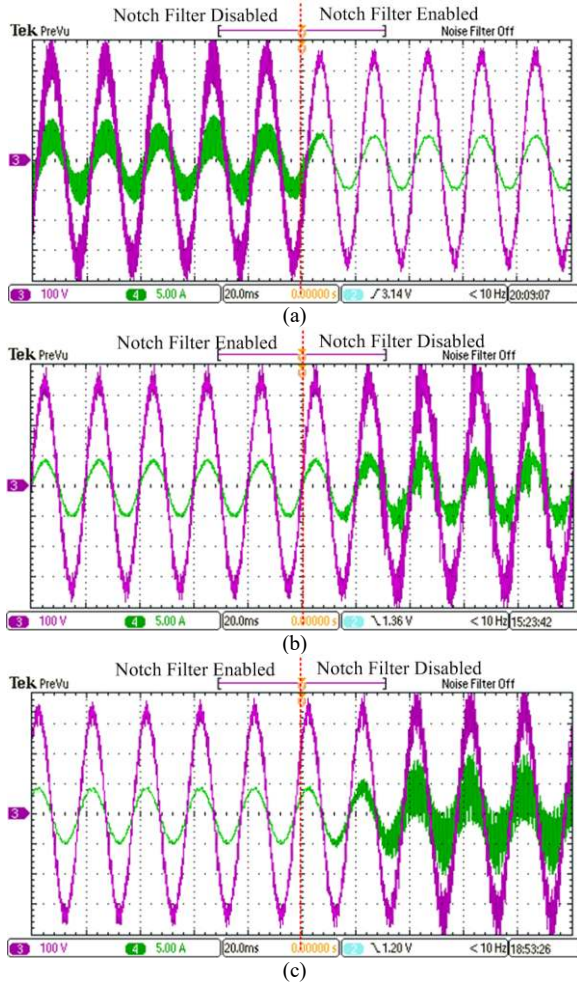
Fig. 15. Performance of the proposed digital notch filter based active damping for a three-phase grid-connected inverter system with an *LCL* filter (phase voltage CH 3: [100 V/div], grid current CH 4: [5A/div], and time [20 ms/div]): (a) using the ICF control with the resonant frequency f_{res} = 2835 Hz, i.e., in the region of ICF II, (b) using the ICF control with the resonant frequency f_{res} = 4222 Hz, i.e., in the region of ICF III, and (c) using the GCF control with the resonant frequency f_{res} = 1377 Hz, i.e., in the region of GCF I.
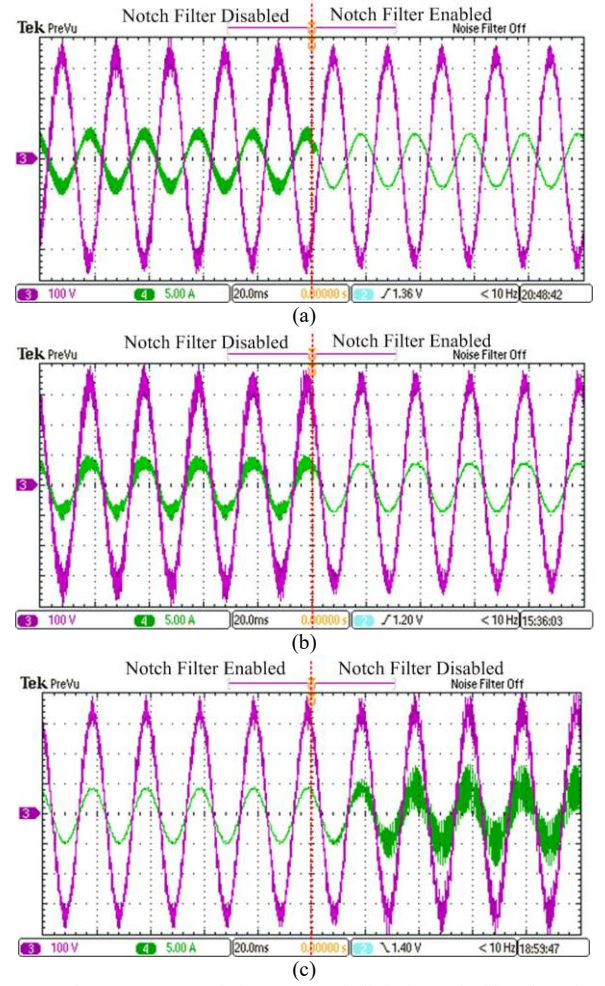

Fig. 16. Robustness tests of the proposed digital notch filter based active damping (phase voltage CH 3: [100 V/div], grid current CH 4: [5 A/div], and time [20 ms/div]): (a) with an additional 1.8 mH inductor per phase using the ICF control, where the resonant frequency f_{res} = 2100 Hz, i.e., in the region of ICF II, (b) with an additional 1.8 mH inductor per phase using the ICF control, where the resonant frequency f_{res} = 3718 Hz, i.e., in the region of ICF III, and (c) with the capacitance being 9.4 μF using the GCF control, where the resonant frequency f_{res} = 1687 Hz, i.e., in the region of GCF I.

grid impedance variations, but it is sensitive to *LCL* parameter negative changes, as discussed in § III. Nevertheless, as it is shown in Fig. 16(c), with the proposed digital notch filter based active damping, the system is stable without oscillations even when the GCF control is employed. However, when the designed notch filter is disabled, as anticipated, the grid currents become resonating, which are demonstrated in Fig. 16(c).

In addition, the entire system with the proposed digital notch filter based active damping is also tested under load transients. Fig. 17 shows the dynamic performance of the entire grid-connected inverter system with either a GCF or an ICF control, where the amplitude of the output currents of the three-phase inverter had experienced a step change from 1 A to 4 A. It can be seen in Fig. 17 that with the proposed digital notch filter based active damping, the grid current can follow the reference without oscillations no matter what current is fed back to the current control loop (i.e., GCF or ICF control). The experimental results shown in Fig. 17 further confirm the robustness and the effectiveness of the proposed digital notch filter based active damping for *LCL* filters in grid-connected applications.

VI. CONCLUSIONS

In this paper, the effectiveness of the conventional notch filter based active damping for *LCL* filters has been explored when considering the sampling and computation process delay in digital control systems and also filter parameter variations. Accordingly, a design method of digital notch filters for robust active damping has been proposed. It has been revealed in this paper that, when the resonant frequency of the *LCL* filter drifts from its designed nominal value, the phase lead or lag introduced by the notch filter that is around the actual resonant frequency may affect the control loop stability. Thus, in the proposed digital notch filter based active damping, the notch frequency is placed on purpose away from the nominal resonant frequency of the *LCL* filter. In that case, the proposed notch filter can provide sufficient phase lead or lag around the resonant frequency to stabilize the control system, contributing to robust active damping. The entire system stability has been investigated in the case of different resonant frequencies induced by grid impedance changes and/or filter parameter
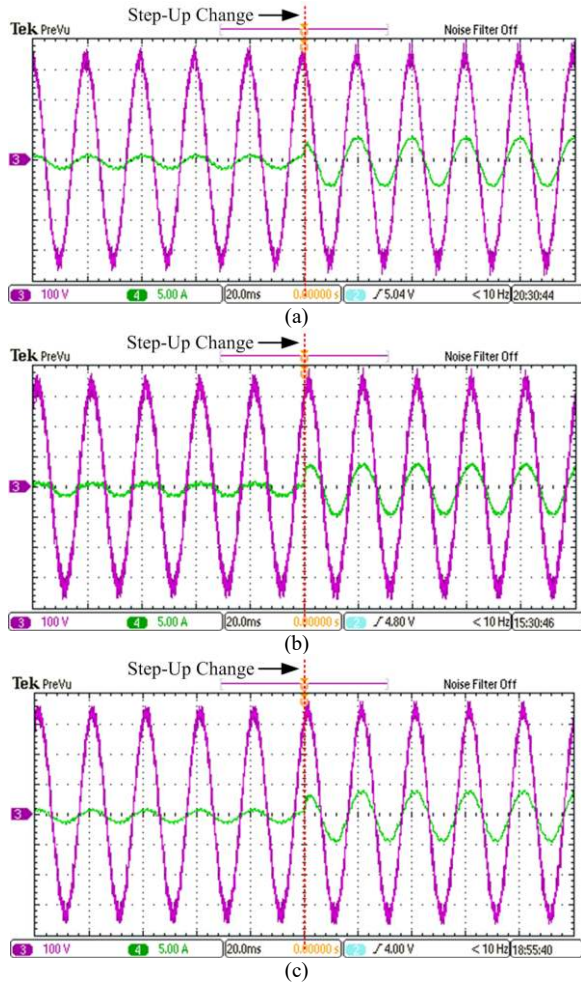
Fig. 17. Dynamic responses of the three-phase systems with the proposed digital notch filter based active damping, where the current reference steps up to 4 A from 1 A (phase voltage CH 3: [100 V/div], grid current CH 4: [5 A/div], and time [20 ms/div]): (a) using the ICF control with the resonant frequency f_{res} = 2835 Hz, i.e., in the region of ICF II, (b) using the ICF control with the resonant frequency f_{res} = 4222 Hz, i.e., in the region of ICF III, and (c) using the GCF control with the resonant frequency f_{res} = 1377 Hz, i.e., in the region of GCF I.

drifting. Both simulations and experiments have verified the effectiveness of the proposed digital notch filter based active damping method in terms of high robustness.

REFERENCES

[1] R. Teodorescu, F. Blaabjerg, M. Liserre, and A. Dell'Aquila, "A stable three-phase *LCL*-filter based active rectifier without damping," in *Proc. of IEEE IAS Annu. Meeting*, pp. 1552-1557, 2003.

[2] J. Dannehl, C. Wessels, and F.W. Fuchs, "Limitations of voltage-oriented PI current control of grid-connected PWM rectifiers with *LCL* filters," *IEEE Trans. Ind. Electron.*, vol. 56, no. 2, pp. 380-388, Feb. 2009.

[3] S. Parker, B. P. McGrath, and D. G. Holmes, "Region of active damping control for *LCL* filters," *IEEE Trans. Ind. Appl.*, vol. 50, no. 1, pp. 424-432, Jan.-Feb. 2014.

[4] J.G. Wang, J. D. Yan, L. Jiang, and J.Y Zou, "Delay-Dependent Stability of Single-Loop Controlled Grid-Connected Inverters with *LCL* Filters," *IEEE Trans. Power Electron.*, vol. 31, no. 1, pp. 734-757, Jan. 2016.

[5] D. Pan, X. Ruan, C. Bao, W. Li, and X. Wang, "Capacitor-current feedback active damping with reduced computation delay for improving ro-

[6] bustness of LCL-type grid-connected inverter," *IEEE Trans. Power Electron.*, vol. 29, no. 7, pp. 3414-3427, Jul. 2014.

[6] C. Bao, X. Ruan, X. Wang, W. Li, D. Pan, and K. Weng, "Step-by-step controller design for LCL-Type Grid-Connected inverter with capacitor-current-feedback active-damping," *IEEE Trans. Power Electron.*, vol. 29, no. 3, pp. 1239-1253, Mar. 2014.

[7] J. Yin, S. Duan, and B. Liu, "Stability Analysis of Grid-Connected Inverter with LCL Filter Adopting A Digital Single-Loop Controller with Inherent Damping Characteristic," *IEEE Trans. Ind. Inform.*, vol. 9, no. 2, pp. 1104-1112, May. 2013.

[8] C. Zou, B. Liu, S. Duan, and R. Li, "Influence of Delay on System Stability and Delay Optimization of Grid-Connected Inverters With LCL Filter," *IEEE Trans. Ind. Inform.*, vol. 10, no. 3, pp. 1775-1784, Aug. 2014.

[9] M. Liserre, A. Dell'Aquila, and F. Blaabjerg, "Stability improvements of an *LCL*-filter based three-phase active rectifier," in *Proc. of IEEE PESC'02*, pp. 1195-1201, 2002.

[10] R.Peña-Alzola, M.Liserre, F.Blaabjerg, R. Sebastián, J. Dannehl, and F. W. Fuchs, "Analysis of the passive damping losses in *LCL*-filter-based grid converters," *IEEE Trans. Power Electron.*, vol. 28, no. 6, pp. 2642-2646, Jun. 2013.

[11] Y. Tang, P. Loh, P. Wang, F. Choo, and F. Gao, "Exploring inherent damping characteristic of *LCL*-filters for three-phase grid-connected voltage source inverters," *IEEE Trans. Power Electron.*, vol. 27, no. 3, pp. 1433-1443, Mar. 2012.

[12] P. A. Dahono, "A control method to damp oscillation in the input LC-filter," in *Proc. of PESC*, vol. 4, pp. 1630-1635, 2002.

[13] X. Wang, F. Blaabjerg, and P. Loh, "Virtual RC Damping of LCL-Filtered Voltage Source Converters with Extended Selective Harmonic Compensation." *IEEE Trans. Power Electron.*, vol. 30, no. 9, pp. 4726-4737, Sep. 2015.

[14] V. Blasko and V. Kaura, "A novel control to actively damp resonance in input *LC* filter of a three-phase voltage source converter," *IEEE Trans. Ind. Appl.*, vol. 33, pp. 542-550, Mar.-Apr. 1997.

[15] R. Pena-Alzola, M. Liserre, F. Blaabjerg, R. Sebastian, J. Dannehl, and F. W. Fuchs, "Systematic Design of the Lead-Lag Network Method for Active Damping in LCL-Filter Based Three Phase Converters," *IEEE Trans. Ind. Informat.*, vol. 10, no.1, pp. 43- 52, Feb. 2014.

[16] R. Pena-Alzola, M. Liserre, F. Blaabjerg, M. Ordonez, and Y. Yang, "LCL-Filter Design for Robust Active Damping in Grid Connected Converters," *IEEE Trans. Ind. Inform.*, vol. 10, no. 4, pp. 2192-2203, Nov. 2014.

[17] Dick, S. Richter, M. Rosekeit, J. Rolink, and R. De Doncker, "Active damping of *LCL* resonance with minimum sensor effort by means of a digital infinite impulse response filter," in *Proc. of EPE*, pp.1-8, 2007.

[18] G. Shen, D. Xu, D. Xi, and X. Yuan, "An improved control strategy for grid-connected voltage source inverters with a LCL filter," *IEEE Trans. Power Electron.*, vol. 23, no. 4, pp. 1899-1906, Jul. 2008.

[19] G. Shen, X. Zhu, J. Zhang, and D. Xu, "A new feedback method for PR current control of LCL-filter-based grid-connected inverter," *IEEE Trans. Ind. Electron.*, vol. 57, no. 6, pp. 2033-2041, Jun. 2010.

[20] W. Gullvik, L. Norum, and R. Nilsen, "Active damping of resonance oscillations in LCL-filters based on virtual flux and virtual resistor," in *Proc. of EPE*. pp. 1-10, 2007.

[21] M. Liserre, A. Dell'Aquilla, and F. Blaabjerg, "Genetic algorithm based design of the active damping for a LCL-filter three-phase active rectifier," *IEEE Trans. Power Electron.*, vol. 19, no. 1, pp. 234-240, Jan. 2003.

[22] J. Dannehl, M. Liserre, and F. Fuchs, "Filter-based active damping of voltage source converters with LCL-filter," *IEEE Trans. Ind. Electron.*, vol. 58, no. 8, pp. 3623-3633, Aug. 2011.

[23] R. Peña Alzola, M. Liserre, F. Blaabjerg, M. Ordonez, and T. Kerekes, "A self-commissioning notch filter for active damping in a three-phase LCL -filter-based grid-tie converter," *IEEE Trans. Power Electron.*, vol. 29, no. 12, pp. 6754–6761, Dec. 2014.

[24] C. Xie, Y. Wang, X. Zhong, and C. Chen, "A novel active damping method for LCL-filter-based shunt active power filter," in *Proc. of IEEE ISIE'12*, pp. 64–69, 2012.

[25] Y. Liu, W. Wu, Y. He, Z. Lin, F. Blaabjerg, Chung, H.S, "An Efficient and Robust Hybrid Damper for LCL - or LLCL -Based Grid-Tied Inverter With Strong Grid-Side Harmonic Voltage Effect Rejection," *IEEE Trans. Indus Electron.*, vol. 63, no. 2, pp. 926-936, Feb. 2016.

[26] S. Zhang, S. Jiang, X. Lu, B. Ge, F. Peng, "Resonance Issues and Damping Techniques for Grid-Connected Inverters With Long Transmission Cable," *IEEE Trans. Power Electron.*, vol.29, no.1, pp. 110-120, Jan. 2014.

[27] W. Yao, Y. Yong, X. Zhang, and F. Blaabjerg, "Digital notch filter based active damping for LCL filters," in *Proc. of APEC*, pp. 2399-2406, 2015.

[28] K. Hirano, S. Nishimura, S.K. Mitra, "Design of Digital Notch filter," *IEEE Trans. Circuits Systems.*, vol. 21, no. 4, pp. 540-546, Jul. 1974.

[29] P.A. Regalia, S.K. Mitra, P.P. Vaidyanathan, "The Digital All-Pass Filter: A Versatile Signal Processing Building Block," in *Proc. of the IEEE*, vol. 76, no. 1, pp. 19-37, Jan. 1988.

[30] A. G. Yepes, F. D. Freijedo, J. Doval-Gandoy, O. Lopez, J. Malvar, and P. Fernandez-Comesana, "Effects of discretization methods on the performance of resonant controllers," *IEEE Trans. Power Electron.*, vol. 25, no. 7, pp. 1692-1712, Jul. 2010.

[31] M. Liserre, R. Teodorescu, and F. Blaabjerg, "Stability of photovoltaic and wind turbine grid-connected inverters for a large set of grid impedance values," *IEEE Trans. Power Electron.*, vol. 21, no. 1, pp. 263-272, Jan. 2006.

[32] Y. Tang, W. Yao, P. C. Loh, and F. Blaabjerg, "Design of LCL-Filters with LCL Resonance Frequencies beyond the Nyquist Frequency for Grid-Connected Converters," *IEEE J. Emerg. Sel. Top. Power Electron.,* vol. 4, no. 1, pp. 3-14, July. 2015.

[33] J. L. Agorreta, M. Borrega, J. Lopez, and L. Marroyo, "Modeling and Control of N-Paralleled Grid Connected Inverters With LCL Filter Coupled Due to Grid Impedance in PV Plants," *IEEE Trans. Power Electron.*, vol.26, no.3, pp.770-785, Mar. 2011.

[34] M. Liserre, F. Blaabjerg, and S. Hansen "Design and Control of an LCL-Filter-Based Three-Phase Active Rectifier," *IEEE Trans. Ind Appl.,* vol. 41, no. 5, pp. 1281-1292, Sep./Oct. 2005.

[35] A. Reznik, M. Simoes, A. Al-Durra, and S. Muyeen, "LCL filter design and performance analysis for grid-interconnected systems," *IEEE Trans. Ind. Appl.,* vol. 50, no. 2, pp. 1225–1232, Mar./Apr. 2014

Xiaobin Zhang received the B.S. and M.S degree in electrical engineering from the School of Automation, Northwestern Polytechnical University, Xi'an, China, in 1983 and 1986 respectively. Since 1986, he has been with School of Automation, Northwestern Polytechnical University Xi'an, China, where he is currently a Professor. His research interests include power electronic control, aircraft power system, multipulse converter, and power decoupling

Wenli Yao (S'14) received the B.S. and M.S degree in electrical engineering from the School of Automation, Northwestern Polytechnical University, Xi'an, China, in 2009 and 2012, where he is currently working toward the Ph.D. degree in power electronics. His research interests include current control, grid connected inverter, multipulse converter, and power decoupling

Frede Blaabjerg (S'86 – M'88 – SM'97 – F'03) was with ABB-Scandia, Randers, Denmark, from 1987 to 1988. From 1988 to 1992, he was a Ph.D. Student with Aalborg University, Aalborg, Denmark. He became an Assistant Professor in 1992, an Associate Professor in 1996, and a Full Professor of power electronics and drives in 1998. His current research interests include power electronics and its applications such as in wind turbines, PV systems, reliability, harmonics and adjustable speed drives.

He has received 15 IEEE Prize Paper Awards, the IEEE PELS Distinguished Service Award in 2009, the EPE-PEMC Council Award in 2010, the IEEE William E. Newell Power Electronics Award 2014 and the Villum Kann Rasmussen Research Award 2014. He was an Editor-in-Chief of the IEEE TRANSACTIONS ON POWER ELECTRONICS from 2006 to 2012. He has been a Distinguished Lecturer for the IEEE Power Electronics Society from 2005 to 2007 and for the IEEE Industry Applications Society from 2010 to 2011. He is nominated in 2014 by Thomson Reuters to be between the most 250 cited researchers in Engineering in the world.

Yongheng Yang (S'12 – M'15) received the B.Eng. degree from Northwestern Polytechnical University, Xian, China, in 2009, and the Ph.D. degree from Aalborg University, Aalborg, Denmark, in 2014.

He was a Post-Graduate with Southeast University, Nanjing, China, from 2009 to 2011. In 2013, he was a Visiting Scholar with the Department of Electrical and Computer Engineering, Texas A&M University, College Station, USA. Since 2014, he has been with the Department of Energy Technology, Aalborg University, where he is currently an Assistant Professor. His research interests are focused on grid integration of renewable systems, power converters design and control, harmonics identification and mitigation, and reliability in power electronics.

He is a Member of the IEEE Power Electronics Society Students and Young Professionals Committee. Dr. Yang serves as a Guest Associate Editor of the IEEE JOURNAL OF EMERGING AND SELECTED TOPICS IN POWER ELECTRONICS special issue on Power Electronics for Energy Efficient Buildings. He also serves as a Guest Editor of *Applied Sciences* special issue on Advancing Grid-Connected Renewable Generation Systems.

Poh Chiang Loh received the B.Eng. and M.Eng. degrees from the National University of Singapore, Singapore, in 1998 and 2000, respectively, and the Ph.D. degree from Monash University, Clayton, VIC, Australia, in 2002, all in electrical engineering.

He was an Assistant Professor with Nanyang Technological University, Singapore, from 2003 to 2009, where he has been an Associate Professor since 2009. In 2005, he was with the University of Hong Kong, Hong Kong, first as a Visiting Staff Member, and then with Aalborg University, Aalborg, Denmark. In 2007 and 2009, he again returned to Aalborg University first as a Visiting Staff Member involved in matrix converters and the inverters, and then as a Guest Control of Grid-Interfaced Member of the Vestas Power Program. Currently, he is a Full Professor with Aalborg University. His current research interests include power electronics, power quality, and micro- grids.